Coupling between crystalline anistropy and spontaneous parity breaking in lamellar eutectic growth

K. Kassner
Institut für Festkörperforschung des Forschungszentrums Jülich, W-517 Jülich, Germany

C. Misbah
Institut Laue-Langevin, Boîte Postale 156X, 38042 Grenoble CEDEX, France
(Received 21 January 1992)

Recently, we demonstrated that the liquid-solid interface of the *isotropic* model of lamellar eutectic growth may undergo a parity-breaking transition from a symmetric to a tilted state. We found that the bifurcation to the asymmetric state is supercritical. Now we have solved the full boundary integral equation of the system assuming *anisotropic* surface tension. We observe that generically the supercritical bifurcation becomes imperfect, as could be expected from a simple phenomenological picture. In order to study whether finite domains of tilted states can exist under these circumstances, we consider a simple model for the coupling between tilt angle and phase dynamics that exhibits an imperfect bifurcation. We find that if the anisotropy is not too strong, the coupling leads to a picture that retains many of the qualitative features of the phenomenological approach given by Coullet, Goldstein, and Gunaratne [Phys. Rev. Lett. **63**, 1954 (1989)] for subcritical bifurcations. Furthermore, we offer a natural explanation for the experimental finding that on creation of a tilted state lamellae of a given grain preferentially tilt in one direction, not in the opposite one.

PACS number(s): 61.50.Cj, 05.70.Fh, 81.30.Fb, 68.70.+w

I. INTRODUCTION

When thin samples of eutectic alloys are submitted to directional solidification, they generally form a periodic array of alternating lamellae of the two solid phases α and β [1–3]. Most of the time, but not always, the orientation of these lamellae is roughly parallel to the direction of growth. The exceptions, termed tilted lamellae, have been known to metallurgists for some 20 years at least [4]. They were often attributed to the underlying crystalline anisotropy and assumed to be associated with the grain structure of the crystal (e.g., through locking on low-energy crystallographic planes). Only after the discovery of parity-breaking cells in directional ordering of a liquid crystal by Simon, Bechhoefer, and Libchaber [5] have inclusions of tilted lamellae in eutectics [6] gained reviewed interest. Soon it became clear [7,8] that the tilt instability of lamellar eutectics does not depend on the presence of crystalline anisotropy. The view that parity breaking is a generic bifurcation scenario has found further support by the observation of similar phenomena in directional viscous fingering [9], where there is no microscopic anisotropy at all.

In all cases, the tilted or asymmetric domains travel laterally with respect to the interface, which shows that there must be a strong coupling between the phase dynamics and the order parameter describing the asymmetry of the pattern (e.g., the tilt angle). A first theory, including this coupling in a phenomenological manner, was put forward by Coullet, Goldstein, and Gunaratne [10]. They suggested that the traveling modes are localized inclusions of a new antisymmetric state resulting from a bifurcation of the underlying symmetric structure. An implication is that there should exist homogeneously tilted states of an infinitely extended front. Since in all experiments up to that time tilted states appeared as small inclusions escorted by wide regions of the symmetric state, it was a natural assumption that the tilt bifurcation be subcritical [10], in accord with the descriptive notion of "solitary modes" brought up by experimentalists [5,6]. As it turns out, however, the bifurcation to tilted states is supercritical. This result, first deduced theoretically [7,8,11], has meanwhile been confirmed [12] in an experiment suggested by us [8], which led to the observation of homogeneously tilted parity-broken states.

Given this state of affairs, theory was left with two puzzles set by experiments: the existence of localized inclusions of tilted states in a matrix of an untilted basic state, in spite of the supercritical nature of the bifurcation, and the fact that it seems experimentally difficult to produce, starting with a given eutectic grain, stable tilted domains with tilt angles of both signs, to be expected for a true symmetry-breaking transition. Only when a tilted domain travels across a grain boundary [13] does it sometimes have the "wrong" tilt direction. The first of these puzzles found a preliminary solution through a calculation by Caroli, Caroli, and Fauve [14]: they showed that the coupling between tilt angle and phase dynamics changes the character of the basic bifurcation (in the isotropic model) such that the qualitative features of the Coullet results [10] remain essentially unaltered. As we shall see, the main effect of anisotropy is to render the supercritical bifurcation imperfect. To some extent, this destruction of the bifurcation reinstitutes the puzzle, because the question arises whether the picture developed by Coullet, Goldstein, and Gunaratne and Caroli, Caroli, and Fauve carries over to the situation of an imperfect bifurcation. We will demonstrate that this is indeed the

case as long as the anisotropy is not too strong. In addition, we will obtain an answer to the second puzzle, i.e., an explanation of the preference given to one tilt direction by the pattern. Our derivation of the fact that the coupling between phase and amplitude transforms the nature of the bifurcation is extremely simple. We thus avoid the relatively heavy propagator formalism of Ref. [14].

Here is a brief survey of the organization of this paper. In Sec. II we give the equations of the full "microscopic" model including surface tension anisotropy. Section III is devoted to a comparison of the bifurcations to tilted states obtained from exact numerical solutions of the isotropic and anisotropic models, respectively. In Sec. IV we present a phenomenological model of the coupling between the asymmetry order parameter (amplitude of the antisymmetric state or tilt angle) and the phase dynamics. The stationary solution of that model will have an imperfect bifurcation similar to the one found numerically. We treat the model in the framework of standard procedures to arrive at a description of domains with constant, increasing, or decreasing width. In Sec. V we discuss the implications of our results.

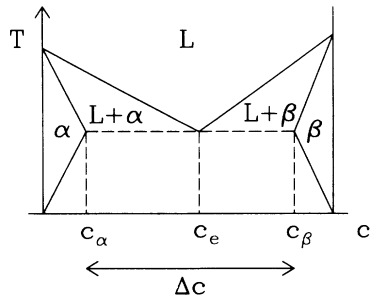

FIG. 1. Phase diagram of eutectics. T is the temperature, c the concentration of one component. The regions L, α, and β correspond to one-phase equilibrium states of the liquid, the solid α, and the solid β phases, respectively. $L+\alpha$ and $L+\beta$ are regions of two-phase equilibrium between the liquid and one solid phase; the true concentrations of the two phases are given by the liquidus and solidus lines (full lines) delimiting these regions. c_e, c_α, and c_β denote the equilibrium concentrations of the liquid and the two solid phases at the triple or eutectic point. Δc is the miscibility gap: $\Delta c = c_\beta - c_\alpha$.

II. MICROSCOPIC MODEL EQUATIONS

Since the model equations have been described elsewhere [15], we will keep their discussion brief and merely emphasize the changes that are needed to include interface tension anisotropy. We consider the standard directional solidification setup with a constant thermal gradient G throughout the sample. The assumptions behind this are that thermal diffusion is fast on the time scale of chemical diffusion, that it proceeds symmetrically in both phases, and that latent-heat production is negligible. We restrict chemical diffusion to the liquid phase, i.e., we work within the one-sided model.

Let c be the concentration, in the liquid, of one of the components of the eutectic, c_e its value at the eutectic point, and Δc the miscibility gap—see the phase diagram given in Fig. 1. In terms of the dimensionless concentration field $u=(c-c_e)/\Delta c$, the diffusion equation for a pattern tilted by an angle ϕ reads

$$\frac{1}{D}\frac{\partial u}{\partial t}=\nabla^2 u+\frac{2}{l}\left[\frac{\partial u}{\partial z}+\tan\phi\frac{\partial u}{\partial x}\right] . \tag{2.1}$$

Coordinates are measured in a frame of reference that is attached to the liquid-solid interface (and is identical with the laboratory frame for $\phi=0$). In this equation, D is the diffusion constant and $l=2D/V$ the diffusion length. V is the velocity by which the sample is pulled (or pushed) along the $-z$ direction. If the tilt angle is nonzero, the interface moves, in the laboratory frame, with velocity $V\tan\phi$ along the x direction.

In the lamellar eutectic problem we can restrict our considerations to one-dimensional front deformations. The boundary conditions for the field $u(x,z;t)$ are then periodicity in the lateral direction

$$u(x+\lambda,z;t)=u(x,z;t) , \tag{2.2}$$

where λ is the (imposed) wavelength of the pattern, constancy of u at infinity

$$u(x,z\to\infty;t)=u_\infty=\frac{c_\infty-c_e}{\Delta c} , \tag{2.3}$$

and local thermal equilibrium at the liquid-solid interface, expressed by the Gibbs-Thomson condition

$$u|_{\text{interface}}=\begin{cases}-\zeta/l_T^\alpha-d^\alpha(\vartheta)\kappa, & \alpha \text{ phase}\\ \zeta/l_T^\beta+d^\beta(\vartheta)\kappa, & \beta \text{ phase} .\end{cases} \tag{2.4}$$

$\zeta(x,t)$ is the position of the interface and $\kappa(x,t)$ its curvature, taken positive where the solid is convex. $l_T^{\alpha/\beta}$ are the thermal lengths, given by

$$l_T^i=\frac{m_i\Delta c}{G}, \quad i=\alpha,\beta \tag{2.5}$$

where m_i is the modulus of the slope of the liquidus line describing coexistence of phase i and the liquid (see Fig. 1). The angle ϑ between the normal vector on the interface and the z direction has been written as an explicit argument of the capillary lengths $d^{\alpha/\beta}$ to emphasize their anisotropy. $d(\vartheta)$ is proportional to the *interface stiffness*, $\gamma(\vartheta)+\gamma''(\vartheta)$, where $\gamma(\vartheta)$ is the angle-dependent surface or interface tension [16]. Any simple model assumption on $\gamma(\vartheta)$ therefore determines $d(\vartheta)$. Assuming fourfold anisotropy

$$\gamma_{ik}=\gamma_{ik}^{(0)}\{1+\bar{\epsilon}_{ik}\cos[4(\vartheta-\vartheta_{ik})]\} , \tag{2.6}$$

where i and k denote either of the three phases α, β, or l, we obtain

$$d^i=d_0^i\{1-\epsilon_{il}\cos[4(\vartheta-\vartheta_{il})]\} , \tag{2.7}$$

with $\epsilon_{il}=15\bar{\epsilon}_{il}$, where d_0^i is given by

$$d_0^i = \frac{\gamma_{il}^{(0)} T_e}{L_i m_i \Delta c}, \quad i=\alpha,\beta \tag{2.8}$$

and T_e is the temperature of three-phase equilibrium, whereas the L_i are effective latent heats per unit volume (for more details see Ref. [15]).

To formulate the condition of mechanical equilibrium at the triple points, we need all three quantities $\gamma_{ik}(\vartheta)$ of Eq. (2.6) plus their derivatives $\gamma'_{ik}(\vartheta)$. In the presence of crystalline anisotropy, the interfaces are subject to, besides the surface tension forces, torques whose contributions are proportional to $\gamma'_{ik}(\vartheta)$. The equilibrium of forces in the triple points can then be written

$$\mathbf{\Gamma}_{\alpha l} + \mathbf{\Gamma}_{\beta l} + \mathbf{\Gamma}_{\alpha\beta} = 0 , \tag{2.9}$$

where the vectors $\mathbf{\Gamma}_{ik}$ are no longer aligned parallel with the phase interfaces; $\|\mathbf{\Gamma}_{ik}\| = [\gamma_{ik}^2(\vartheta) + \gamma_{ik}'^2(\vartheta)]^{1/2}$ and the angle between $\mathbf{\Gamma}_{ik}$ and $\boldsymbol{\gamma}_{ik}$ is given by $\Delta\vartheta_{ik} = \arctan(\gamma'_{ik}/\gamma_{ik})$.

Finally, local mass conservation at the interface provides us with an additional equation

$$-D\frac{\partial u}{\partial n} = \begin{cases} [(1-k_\alpha)u + \delta]v_n, & \alpha \text{ phase} \\ [(1-k_\beta)u + \delta - 1]v_n, & \beta \text{ phase} \end{cases} \tag{2.10}$$

where k_α and k_β are the partition coefficients, here simply expressible as the ratios of the slopes of the liquidus and solidus lines in Fig. 1, and $\delta = (c_e - c_\alpha)/\Delta c$ is the reduced miscibility gap of the α phase. $v_n = (2D/l + \dot{\zeta})n_z$ is the normal velocity of the interface. The normal vector $\mathbf{n}$ points from the solid into the liquid. In Eq. (2.10), an additional capillary length d_0^c has been neglected—it is small for eutectics with small temperature gap $m_i \Delta c$, such as the plastic crystal CBr_4-C_2Cl_6 used frequently in experiments [15].

For *stationary* solutions to the set of equations (2.1)–(2.4) the diffusion equation (2.1) reduces to an elliptic equation. Taken together, boundary conditions (2.4) and (2.10) seem to overdetermine the elliptic problem, which they would indeed *for prescribed interface position.* However, $\zeta(x)$ is a *free boundary;* it is actually the quantity for which the equations are to be solved—and in general one cannot expect the full set of boundary conditions to be satisfied for more than a discrete set of solutions.

III. THE IMPERFECT BIFURCATION

The numerical procedure, which is based on the conversion of the equation of motion into a boundary integral formulation, has been explained in detail previously [15]. Therefore, we just give the results obtained by the method.

In Figs. 2–4 we compare two tilted solutions to the anisotropic problem with one that corresponds to isotropic surface tension. While the anisotropy *is* visible in the interface shape, the deformations it creates are not pronounced, unless it is very strong. Note that the maximum meaningful amplitude ϵ of the anisotropy is one, and to see a strong deviation we have to go beyond

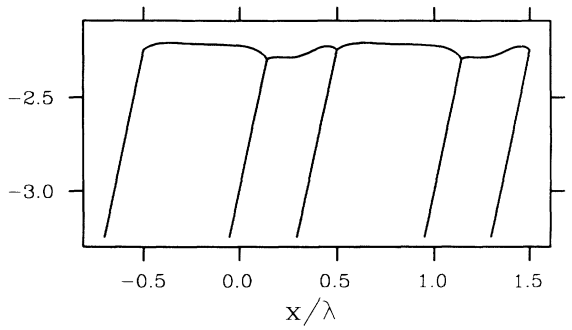

FIG. 2. Tilted solution of isotropic model ($\varphi = 11.5°$). Parameters in time units of D/l^2 and length units of l_T (for the conversion to physical units, see, e.g., Ref. [15]): $V = 27.7$, $\lambda = 0.0082$, $d_0^\alpha = 2\times10^{-5}$, $d_0^\beta = 5\times10^{-6}$, $k_\alpha = 0.99$, $k_\beta = 1.04$, $\delta = 0.3$, $u_\infty = 0.05$.

$\epsilon \approx 0.6$. There is also some dependence on the angles ϑ_{ik}—the deviation from the isotropic profile becomes larger as the ϑ_{ik} increase.

In Figs. 5–7, the tilt angle as a function of the velocity at a fixed wavelength is displayed for three different situations. Figure 5 is the isotropic case and we see the normal bifurcation discussed recently [8]. A tilt angle $\phi = 0$ corresponds to an axisymmetric solution. Note that axisymmetric solutions do not extend to arbitrarily large velocities. They cease to exist at a fold singularity [15]—the symmetric branch of the bifurcation diagram folds back onto itself.

Figure 6 displays a nongeneric case of anisotropy. All three angles $\vartheta_{\alpha l}$, $\vartheta_{\beta l}$, and $\vartheta_{\alpha\beta}$ in (2.6) and (2.7) have been set equal to zero, which means that the anisotropies of capillary lengths and interface tensions are compatible with the axisymmetry of the basic solutions. As a consequence, the character of the bifurcation is not changed. The main effect of anisotropy in this case is to soften the bifurcation.

In Fig. 7 we have still kept the "directors" of the anisotropies of the three phases aligned, but now they are not parallel to the growth axis anymore, i.e., we have set $\vartheta_{\alpha l} = \vartheta_{\beta l} = \vartheta_{\alpha\beta} \neq 0$. This is an example for the generic case, with crystalline anisotropy breaking the original

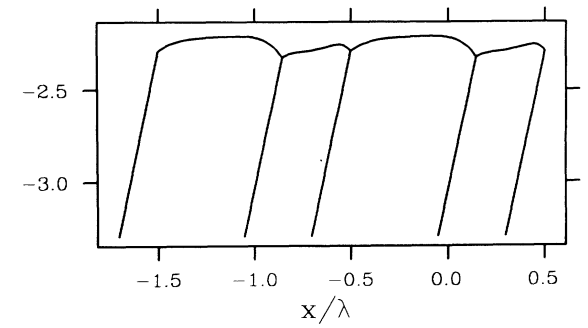

FIG. 3. Tilted solution with anisotropy. $\epsilon_{\alpha l} = \epsilon_{\beta l} = 0.6$, $\epsilon_{\alpha\beta} = 0.1$ $\vartheta_{\alpha l} = \vartheta_{\beta l} = \vartheta_{\alpha\beta} = 0.2$, $\lambda = 0.0071$, other parameters as in Fig. 2. Tilt angle 11.5°.

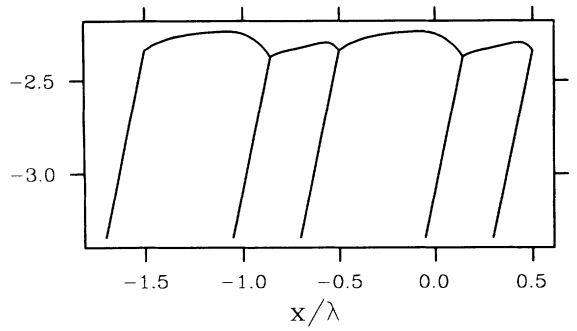

FIG. 4. Tilted solution with anisotropy. $\epsilon_{\alpha l}=\epsilon_{\beta l}=0.75$, $\epsilon_{\alpha\beta}=0.1$, $\vartheta_{\alpha l}=\vartheta_{\beta l}=\vartheta_{\alpha\beta}=0.2$, $\lambda=0.0066$, other parameters as in Fig. 2. Tilt angle 11.5°.

symmetry of the problem. In this situation, no strictly symmetric solutions will exist. The plot of the tilt angle as a function of velocity shows that the bifurcation is destroyed—there are now two independent branches of solutions. The question arises then whether or not the statements about the dynamical evolution of tilted domains that have been made in the past and were based on the assumption of either a subcritical [10] or a supercritical [14] bifurcation are still true in this more complicated situation.

Obviously, the distinction is now no longer between tilted asymmetric and untilted symmetric solutions. Almost all solutions are tilted. There are some with zero tilt angle (two in Fig. 7), but of course the corresponding solutions are not symmetric. There is no true symmetry breaking anymore, rather one has to distinguish between weakly tilted solutions (tilt angles typically 5° or less) and strongly tilted ones, and the transition from the former to the latter is smooth. Furthermore, lamellae tilted to the left and the right have different stabilities, so that one expects preferred tilt orientations to appear.

These results are corroborated by experiments [13] which show that there is a distribution of nonzero (small)

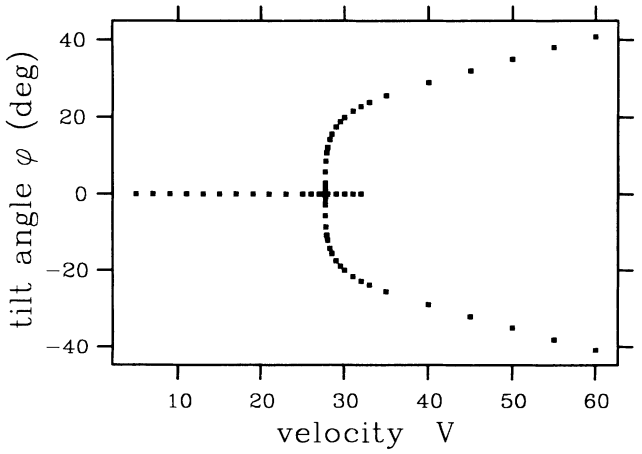

FIG. 5. Numerically calculated bifurcation diagram of the tilt angle for isotropic surface tension. $\lambda=0.008$, material parameters as in Fig. 2.

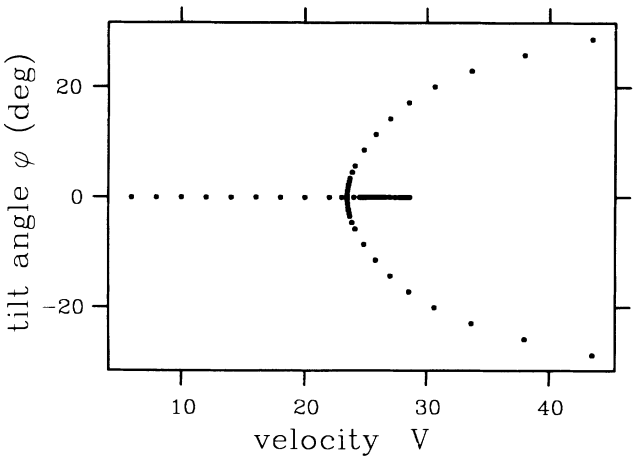

FIG. 6. Numerically calculated bifurcation diagram of the tilt angle for anisotropic surface tension. $\lambda=0.008$, $\epsilon_{\alpha l}=\epsilon_{\beta l}=0.4$, $\epsilon_{\alpha\beta}=0.1$, $\vartheta_{\alpha l}=\vartheta_{\beta l}=\vartheta_{\alpha\beta}=0.0$, material parameters as in Fig. 2.

tilt angles in regular lamellar growth. In addition, there is a correlation between tilt angles and the underlying grain structure [17].

IV. MODEL FOR THE COUPLING BETWEEN PHASE DYNAMICS AND ANTISYMMETRY ORDER PARAMETER

We now construct a simplified model that captures the essential features of the imperfect bifurcation in the vicinity of the transition from weakly to strongly tilted solutions. The system is described by the two coupled equations

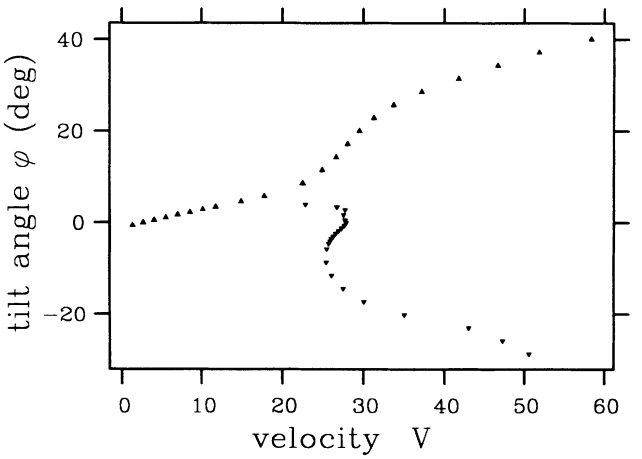

FIG. 7. Numerically calculated bifurcation diagram of the tilt angle for anisotropic surface tension. The tip-up and the tip-down triangles correspond to the two branches. $\lambda=0.008$, $\epsilon_{\alpha l}=\epsilon_{\beta l}=0.4$, $\epsilon_{\alpha\beta}=0.1$, $\vartheta_{\alpha l}=\vartheta_{\beta l}=\vartheta_{\alpha\beta}=0.2$, material parameters as in Fig. 2. Note that the tilt angle is zero at $V=2.6$ and 27.8. These two points constitute boundaries for the branch pieces in which the tilt angle and the antisymmetric part of the profile can be considered to behave qualitatively the same.

$$A_t = A_{xx} + \mu A - \alpha A^3 + \epsilon A \Phi_x + \gamma A A_x + \nu \ , \quad (4.1)$$

$$\Phi_t = D' \Phi_{xx} + \omega A \ . \quad (4.2)$$

In these equations, A is the amplitude of the antisymmetric part of the front profile $\zeta(x)$ and Φ is the phase of the profile,

$$\zeta(x) = S\zeta_S(x+\Phi) + A\zeta_A(x+\Phi) \ , \quad (4.3)$$

where $\zeta_S(x) = \zeta_S(-x)$, $\zeta_A(x) = -\zeta_A(-x)$, and $S(x)$, $A(x)$, and $\Phi(x)$ are slowly varying quantities. [$S(x)$ is the amplitude of the symmetric part of the profile and will not be considered here.]

Equations (4.1) and (4.2) constitute a truncated gradient expansion constructed from symmetry arguments. Terms such as $\Phi_{xx}, \Phi_x \Phi_{xx}$ in (4.1) and A_{xx}, AA_x, $A\Phi_x$, etc. in (4.2) are allowed by symmetry but will not be considered here. It has been shown in Ref. [14] that it is legitimate to truncate the expansion if the conditions $D' \ll 1$ and $\epsilon\omega = O(|\mu|)$ are met, which we will henceforth assume. While it seems likely that the first of these conditions is fulfilled in eutectics due to the slowness of phase diffusion [13], the second assumption becomes problematic, as soon as the bifurcation point is approached very closely, because usually ϵ and ω are not taken to depend on μ. However, our main concern will not be the "bifurcation point" itself but the region about a "Maxwell-like" point below the bifurcation, where such a relation of magnitudes is conceivable.

In a certain range about the crossover between small and large tilt angles, A may, instead of being considered the amplitude of the antisymmetric part of the profile, be identified with the tilt angle itself. This identification is not completely equivalent, because here, other than in the isotropic case, a zero tilt angle does not guarantee a symmetric profile. However, the difference between the two interpretations of A becomes important only very far from the bifurcation (see Fig. 7).

Equations (4.1) and (4.2) have been considered before, but without the ν term [14]. For $\nu = 0$, they are invariant under the two groups of transformations $(x, A, \Phi) \rightarrow (-x, -A, -\Phi)$ and $\Phi \rightarrow \Phi + \text{const}$. A nonzero value of ν, intended to represent the influence of anisotropy, breaks the first of these symmetries.

We easily see from Eq. (4.1) that for $\mu \rightarrow 0$ the amplitude scales with the strength of crystalline anisotropy as $A \sim |\nu|^{1/3}$. This can be thought of as a measure of the "imperfection force." Furthermore, the "susceptibility" for the linear response diverges as $1/\mu$. These features are well known in Landau's theory of phase-transition phenomena, where A may represent, for example, the magnetization, while ν mimics the external magnetic field.

In Fig. 8 we show the behavior of a stationary and spatially homogeneous solution to (4.1), with $\Phi = \text{const} \times t$, as a function of μ. There are two nonoverlapping solution branches, resembling the picture of the imperfect bifurcation in Fig. 7. The main difference is that the branch below the μ axis in Fig. 8 has an upper part that extends to infinity, whereas the corresponding piece in Fig. 7 bends back towards smaller V values on account of the fold singularity [15], which is still present in the anisotropic case. Nevertheless, up to the turning point corresponding to the fold (i.e., well beyond the point corresponding to $\mu = 0$), the model equations (4.1) and (4.2) reproduce the structure of the imperfect bifurcation of the real system, if μ is identified with a parameter that increases with V. Since we do not have the data to calculate the coefficients of amplitude equations from the full model, any results obtained from these equations will be qualitative only. Therefore, an overall agreement of the topology and general behavior of the bifurcation in the range of interesting parameters should be sufficient for our purposes. From similarity considerations [15,18,19] we infer that the parameter of the full model being related monotonously to μ is, in a wide range of experimental situations, given by

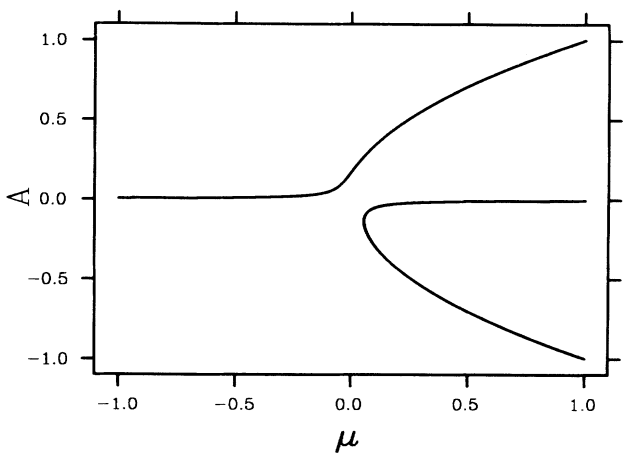

FIG. 8. Bifurcation diagram corresponding to homogeneous solutions of (4.1) and (4.2). Parameters: $\alpha = 1$, $\nu = 0.005$. The coordinates of the turning point are $\mu = 3(\nu/2)^{2/3}$, $A = -(\nu/2)^{1/3}$.

$$\frac{1}{\sigma} = \frac{\lambda^2 V}{2Dd_0} \quad (4.4)$$

(where d_0 is the prefactor of one of the capillary lengths in Eq. (2.7) [15]), i.e., extended tilted states appear when σ falls below a critical value σ_c. Increasing μ at constant Φ_x would then correspond to an increase in the growth velocity V at constant wave vector. Since an increase in λ at constant V must have the same effect, and increasing λ means decreasing Φ_x (which is the local wave vector) the *sign of ϵ in Eq. (4.1) has to be negative.*

The term ωA in (4.2) describes the drift of the pattern along the front. In the absence of anisotropy, the bifurcation is supercritical, so α must be positive. It is then possible to rescale time, space, and the parameters ϵ, γ, and ω such that the prefactor of A^3 in Eq. (4.1) is 1. From now on we will therefore assume $\alpha = 1$, without restricting the generality of our results.

A first step toward a description of inclusions having one tilt angle in a matrix with a different tilt angle is to consider the motion of a boundary separating two domains with different tilt angles. Such a boundary will

be described by a kink solution to Eqs. (4.1) and (4.2).

Assuming that there exist solutions traveling at constant velocity v in the x direction, i.e., $A=A(x-vt)$, $\Phi=v_0 t+\tilde{\Phi}(x-vt)$, we substitute $X=x-vt$ in (4.2), transforming that equation into

$$\frac{v_0}{v}-\tilde{\Phi}_X=l_\Phi\tilde{\Phi}_{XX}+\frac{\omega}{v}A\ , \tag{4.5}$$

where $l_\Phi=D'/v$ is the diffusion length for phase diffusion. (We assume the phase-diffusion coefficient D' to be positive.) If $\tilde{\Phi}_X$ and its derivative are assumed to vanish at infinity, this immediately gives $v_0=\omega A|_{t=-\infty}\equiv\omega A_\infty$. Since phase diffusion is slow in eutectics, it is reasonable to assume l_Φ to be small in comparison with the Landau-Ginzburg length $|\mu|^{-1/2}$, an assumption that will be justified in more detail below [in the isotropic case, both quantities diverge as $(V-V_c)^{-1/2}$ close to the bifurcation]. In a first approximation, we can therefore neglect the l_Φ term in (4.5) to obtain

$$\Phi_x(X)=\tilde{\Phi}_X=\frac{\omega}{v}[A_\infty-A(X)]\ , \tag{4.6}$$

which on differentiation with respect to X gives $\tilde{\Phi}_{XX}=-(\omega/v)A_X$. This is plugged back into (4.5) to provide the next-order approximation

$$\Phi_x(X)=\frac{\omega}{v}[A_\infty-A(X)+l_\Phi A_X]\ . \tag{4.7}$$

Inserting this expression into (4.1) we arrive at

$$A_{XX}+[v+(\gamma+\rho l_\Phi)A]A_X+\frac{dU}{dA}=0\ , \tag{4.8}$$

with

$$U(A)=-\tfrac{1}{4}A^4-\tfrac{1}{3}\rho A^3+\tfrac{1}{2}\bar{\mu}A^2+\nu A+\text{const} \tag{4.9}$$

and

$$\rho=\frac{\epsilon\omega}{v},\quad \bar{\mu}=\mu+\rho A_\infty\ . \tag{4.10}$$

The coupling to the phase has changed the "potential," which in the original equation (4.1) was $U_0(A)=-\frac{1}{4}A^4+\frac{1}{2}\mu A^2+\nu A$ into $U(A)$, containing a v-dependent cubic term. Note that to obtain this result, we did not need to use any propagator formalism [14].

Moving domain boundaries to be represented by kink solutions will connect regions of different amplitudes, each of which is roughly constant. These amplitudes are given by the positions of the extrema of U, i.e., by

$$\frac{dU}{dA}=-A^3-\rho A^2+\bar{\mu}A+\nu=0\ . \tag{4.11}$$

Let us first assume isotropic interface tensions, i.e., $\nu=0$, which will turn out to be a useful reference situation. Then one obvious real solution is $A=0$, and the existence and values of the two others are determined by a quadratic equation. If we set $A_\infty=0$ (which corresponds to a symmetric initial state at $t=-\infty$), the condition for this equation to have (two) real solutions becomes

$$\mu>-\frac{\rho^2}{4}=-\frac{\epsilon^2\omega^2}{4v^2}\ , \tag{4.12}$$

i.e., moving asymmetric states can already exist for $\mu<0$ [20]. Plotting the solutions to Eq. (4.11) with $\nu=0$ as a function of μ, we obtain Fig. 9, showing that the initial direct bifurcation has changed into a transcritical one, which allows the simultaneous existence of linearly stable symmetric and asymmetric solutions below $\mu=0$.

We now turn to the case $\nu\neq0$. The condition for the cubic equation (4.11) to have three real roots is [21]

$$q^3+r^2\leq0\ , \tag{4.13}$$

where

$$q=-\tfrac{1}{3}\bar{\mu}-\tfrac{1}{9}\rho^2\ , \tag{4.14}$$

$$r=\tfrac{1}{6}(-\bar{\mu}\rho+3\nu)-\tfrac{1}{27}\rho^3\ . \tag{4.15}$$

After some algebra, the inequality (4.13) reduces to

$$\bar{\mu}^3+\tfrac{1}{4}\rho^2\bar{\mu}^2+\tfrac{9}{2}\nu\rho\bar{\mu}+\nu\rho^3-\tfrac{27}{4}\nu^2\geq0\ . \tag{4.16}$$

Given ρ and ν, this is a cubic inequality for $\bar{\mu}$. Basically two situations can arise: either the cubic equation obtained by replacing the inequality with an equality has one or it has three real roots.

In the first case, if μ_1 is the root, the inequality (4.16) will hold for $\bar{\mu}\geq\mu_1$ and fail to hold for $\bar{\mu}<\mu_1$. That is we have only one solution to Eq. (4.11) if $\bar{\mu}<\mu_1$ and three if $\bar{\mu}\geq\mu_1$. Then the bifurcation scheme either looks like Fig. 8 and there are *no* μ values for which a weakly and a strongly tilted domain can both be linearly stable. Or it takes the appearance of Fig. 10, in which small and large tilt angles *can* coexist below $\bar{\mu}=0$ but have opposite sign.

In the second case, if we order the roots according to $\mu_1\geq\mu_2\geq\mu_3$, the inequality (4.16) will hold for $\bar{\mu}\geq\mu_1$ and $\mu_2\geq\bar{\mu}\geq\mu_3$ but not for $\mu_1>\bar{\mu}>\mu_2$ and $\mu_3>\bar{\mu}$. If μ_1 happens to be equal to μ_2, we have the case of Fig. 9, where the range of coexistence of three solutions to Eq. (4.11)

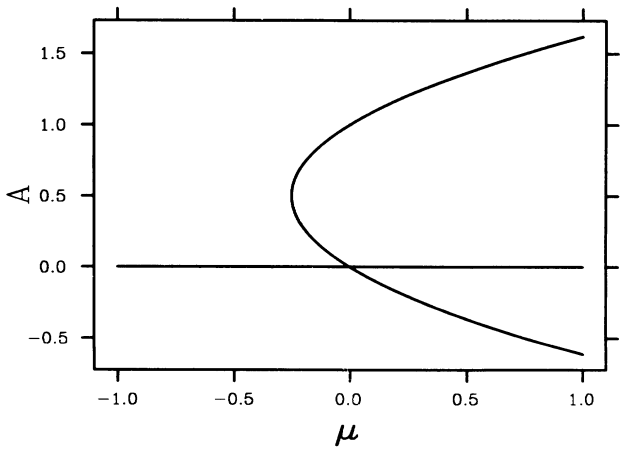

FIG. 9. Transcritical bifurcation corresponding to the potential given in (4.9) for $\nu=0$, $\rho=-1$. Coordinates of the turning point: $\mu=-\rho^2/4$, $A=-\rho/2$.

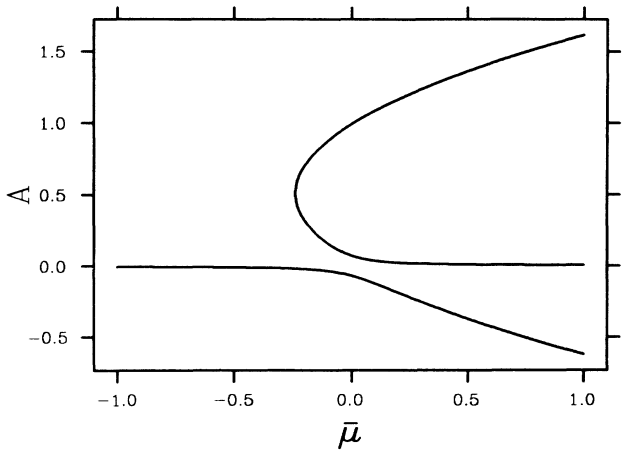

FIG. 10. Bifurcation corresponding to $U(A)$ for $v=-0.005$, $\rho=-1$. To lowest order in v, the turning point is located at $\bar{\mu}=-\rho^2/4+2v/\rho$, $A=-\rho/2-2v/\rho^2$.

extends beyond $\mu_1=\mu_2=0$ down to $\mu_3=-\frac{1}{4}\rho^2$ (and two solutions become degenerate at $\bar{\mu}=\mu_1$). A typical picture for the generic case is given in Fig. 11—there the upper branch of the imperfect bifurcation looks like a true subcritical bifurcation.

The general picture is therefore that whenever there are three solutions to the pertinent cubic equation [obtained from (4.16)] we know for sure that there is a region of coexistence of weakly and strongly tilted states, whereas in the case of only one solution further investigation is necessary to decide whether this is true. It is natural to first concentrate on the case where the decision is easy. The question is then for which parameter combinations ρ, v will there be three solutions. The answer is again given by criterion (4.13), this time with

$$q=\tfrac{3}{2}v\rho-\tfrac{1}{144}\rho^4 , \tag{4.17}$$

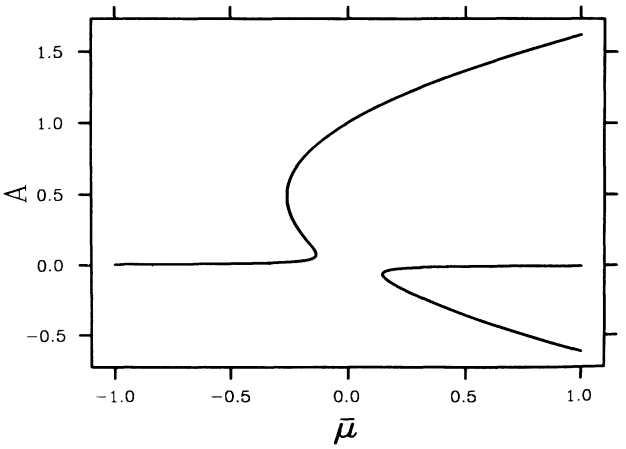

FIG. 11. Bifurcation corresponding to $U(A)$ for $v=0.005$, $\rho=-1$. There are three turning points; their perturbative coordinates are $\bar{\mu}_1=-\rho^2/4+2v/\rho$, $\tilde{A}_1=-\rho/2-2v/\rho^2$; $\bar{\mu}_{2/3}=\mp\sqrt{2|\rho v|}$, $\tilde{A}_{2/3}=\pm\sqrt{|v/2\rho|}$.

$$r=-\tfrac{5}{16}v\rho^3+\tfrac{27}{8}v^2-\frac{1}{2^6\times 3^3}\rho^6 . \tag{4.18}$$

We obtain

$$q^3+r^3=(\tfrac{3}{2})^6v^4+\tfrac{1}{4}(\tfrac{3}{2})^4\rho^3v^3+\tfrac{3}{64}\rho^6v^2+\frac{1}{2^6\times 3^3}\rho^9v , \tag{4.19}$$

which is a fourth-order polynomial in v.

For small enough $|v|$, the linear term will be dominant, and if we choose the sign of v opposite to that of ρ, we immediately get $q^3+r^2<0$, which demonstrates that with small anisotropy the inverted part of the bifurcation as shown in Fig. 11 exists for one sign of v. From continuity arguments, we then conclude that for the other sign of v we must have the situation depicted in Fig. 10.

A. Constant-width domains

Our description of domains with one tilt angle moving in a matrix with another angle will consist of a sequence of two kink solutions (of opposite orientation) modeling the boundaries of the domain. We consider the case $v>0$, i.e., the front and back domain walls are synonymous with right and left kink solutions. They are assumed to be so far apart that they do not interact.

Then from the conditions for a *constant-width* domain to exist we will be able to calculate the Maxwell point $\bar{\mu}^*$ of equal stability of both phases. If we treat, as usual, the dissipative part of Eq. (4.8) as a perturbation, these conditions are (i) that $U(A)$ has to have two maxima of the same height (and this height must be zero) and (ii) that the integral over the dissipation vanishes,

$$\int_{-\infty}^{\infty} dX \left[v+\left[\gamma+\frac{\epsilon\omega D'}{v^2} \right] A \right] A_X^2=0 . \tag{4.20}$$

The equation determining the extrema of U is (4.11). In the range of interest it has three solutions A_1, A_2, A_3, two of which are maxima. Equating $U(A_1)$ with $U(A_3)$ and substituting third and fourth powers of A_1 and A_3 by lower ones using (4.11), we obtain an expression which is quadratic in A_1 and A_3

$$(A_1^2-A_3^2)(\tfrac{1}{12}\rho^2+\tfrac{1}{4}\bar{\mu})+(A_1-A_3)(-\tfrac{1}{12}\rho\bar{\mu}+\tfrac{3}{4}v)=0 . \tag{4.21}$$

Factoring out A_1-A_3 we get a formula for A_1+A_3 which immediately allows us to solve for A_2 via Vieta's theorem ($A_1+A_2+A_3=-\rho$),

$$A_2=\frac{-\rho^3-4\bar{\mu}\rho+9v}{\rho^2+3\bar{\mu}} . \tag{4.22}$$

Moreover, since A_2 is a solution to (4.11), plugging (4.22) into that equation provides a relation between ρ, v, and $\bar{\mu}$, which after some lengthy algebra takes the form

$$\rho x^4-(\tfrac{7}{3}\rho^3+\tfrac{3}{4}R+\tfrac{9}{4}v)x^3+\tfrac{27}{4}R\rho^2x^2-\tfrac{27}{4}R^2\rho x+\tfrac{9}{4}R^3=0 , \tag{4.23}$$

where $x=3\bar{\mu}+\rho^2$ and $R=\frac{1}{3}\rho^3+9\nu$. All the $\bar{\mu}$ dependence is in x, therefore, given ν and ρ, this is a fourth-order algebraic equation for $\bar{\mu}$. However, there are not four Maxwell points, so some of the solutions to (4.23) must be spurious. In fact, the conditions leading to (4.23), namely equal potential value in two points with vanishing first derivative, are fulfilled trivially whenever $U(A)$ has a point of inflexion with horizontal tangent, which always signifies a transition from a situation with a single real root of (4.11) to one with three, or vice versa. But the $\bar{\mu}$ values, at which this happens, are given by the third-order equation corresponding to (4.16). Hence we simply can divide the quartic polynomial of (4.23) by the cubic one of (4.16) to eliminate the undesired roots. The result is

$$\bar{\mu}^*=-\tfrac{2}{9}\rho^2+3\frac{\nu}{\rho}\ , \tag{4.24}$$

and although it is exact, it can also be derived via first-order perturbation theory in ν, because ν appears only linearly. Clearly, (4.24) reduces to the result of Ref. [14] for $\nu=0$. At the Maxwell point, the three solutions to (4.11) are given by

$$A_{1/3}=-\tfrac{1}{3}\rho\mp A^+\ , \tag{4.25}$$

$$A_2=-\tfrac{1}{3}\rho\ , \tag{4.26}$$

where

$$A^+=\frac{|\rho|}{3}\left[1+27\frac{\nu}{\rho^3}\right]^{1/2}=\left[-\frac{\bar{\mu}^*}{2}+\frac{9}{2}\frac{\nu}{\rho}\right]^{1/2}\ . \tag{4.27}$$

Setting $Z(X)=(A+\frac{1}{3}\rho)/A^+$ we can rewrite dU/dA as

$$\frac{dU}{dA}=\frac{1}{A^+}\frac{dU}{dZ}=-A^{+3}Z(Z^2-1)\ , \tag{4.28}$$

and the equation of motion (4.8) reduces on omission of the dissipation term to

$$Z_{XX}-A^{+2}Z(Z^2-1)=0\ . \tag{4.29}$$

The pertinent solutions to this equation are trajectories joining small-amplitude regions ($A=A_1$) at $X=-\infty$ to large-amplitude ones ($A=A_3$) at $X=\infty$, and vice versa. They are given by

$$Z(X)=\pm\tanh\left[\frac{1}{\sqrt{2}}A^+(X-X_0)\right]\ , \tag{4.30}$$

where X_0 is an arbitrary shift of the argument. The plus sign corresponds to the left kink, the minus sign to the right one.

We are now in a position to perform the integral (4.20), which yields a condition for the velocity in terms of the model parameters

$$v^4-\tfrac{1}{3}\epsilon\omega\gamma v^2-\tfrac{1}{3}\epsilon^2\omega^2D'=0\ , \tag{4.31}$$

solved by

$$v^{*2}=\tfrac{1}{6}\epsilon\omega\gamma\left[1+\mathrm{sgn}(\epsilon\omega\gamma)\left[1+12\frac{D'}{\gamma^2}\right]^{1/2}\right]\ . \tag{4.32}$$

This result is identical to the one obtained by Caroli, Caroli, and Fauve [14], i.e., to first order in the dissipation, ν does not appear in the formula and the velocity at the Maxwell point is independent of crystalline anisotropy. From a short calculation, one concludes that the assumption $l_\Phi \ll |\mu|^{-1/2}$, on which the *slaving* (4.7) of the phase to the amplitude is based, is justified only if $\epsilon\omega\gamma>0$, i.e., $\mathrm{sgn}(\epsilon\omega\gamma)=1$.

For definiteness, we will from now on assume that ν is positive and ρ negative, i.e., $\omega/v>0$. With $\epsilon\omega\gamma>0$ this implies $\gamma<0$. Then it follows from (4.25) and (4.26) that the amplitude of a kink solution at μ^* is always positive. This agrees with Ref. [10], stating that at μ^* a kink with positive amplitude moves to the right, if $\omega>0$. Of course, we could equally well consider negative ν values and positive ρ values; in that case the amplitude would be negative. If ν and ρ have the same sign, the amplitudes on both sides of a domain wall have opposite signs. Our final results obtained below will be true for all combinations of signs. We choose one here in order to make sign discussions easier.

With (4.32), the values of all other quantities are also determined in terms of the basic parameters

$$\rho^*=\frac{\epsilon\omega}{v^*}\ , \tag{4.33}$$

$$A^+=\frac{1}{3}\left|\frac{\epsilon\omega}{v^*}\right|\left[1-27\left|\nu\left[\frac{v^*}{\epsilon\omega}\right]^3\right|\right]^{1/2}\ , \tag{4.34}$$

$$\mu^*=-\frac{2}{9}\left[\frac{\epsilon\omega}{v^*}\right]^2+3\nu\frac{v^*}{\epsilon\omega}+\frac{1}{3}\left[\frac{\epsilon\omega}{v^*}\right]^2\left\{1-\left[1-27\left|\nu\left[\frac{v^*}{\epsilon\omega}\right]^3\right|\right]^{1/2}\right\}\ . \tag{4.35}$$

The last equation is a consequence of setting $A_\infty=A_1$ in (4.10). Obviously, for this solution to be meaningful we must require $|\nu|<\frac{1}{27}|\epsilon\omega/v^*|^3$.

Since we know how μ is related qualitatively to the parameter σ [see Eq. (4.4)], we can restate our result in terms of physical quantities. Let us first recall that in the isotropic reference case there is, for each wavelength λ, a *critical* velocity $V_c(\lambda)$, above which extended tilted states exist. In the anisotropic case there is strictly speaking no critical point. Nevertheless, a velocity $V_c(\lambda)$ separating weakly and strongly tilted solutions can still be identified—it corresponds to the point $\bar{\mu}=0$ in the bifurcation diagram.

Our calculations then indicate that, given the wavelength λ of a weakly tilted pattern, it is possible to choose a pulling velocity $V^*(\lambda)$ (thereby adjusting the amplitude to A_1) at which inclusions of a strongly tilted pattern can exist within the weakly tilted one. These inclusions will neither expand nor shrink; both their front and back walls move at a fixed lateral velocity v^*; furthermore, $V^*(\lambda)$ is *smaller* than the velocity $V_c(\lambda)$, above which infinitely extended domains with large tilt are possible. Because $\Phi_X(-\infty)=0$ for the left kink [see Eq. (4.7)], the passage of such an inclusion does not affect the wavelength of the weakly tilted pattern.

On the other hand, given the growth velocity of a weakly tilted pattern, μ^* defines a wavelength $\lambda^*(V)$ at which constant-width inclusions traveling with velocity v^* are possible; again λ^* is smaller than the wavelength λ_c for which V is the critical velocity. However, it is more interesting to determine the relation between the wavelengths $\lambda_s=\lambda^*$ and λ_l of the regions with small and large tilt angle, respectively. Equation (4.7) gives (applied to the right kink) the difference between the wave numbers

$$q_l-q_s=\Phi_X(-\infty)-\Phi_X(\infty)=-2\frac{\omega}{v^*}A^+<0\ , \tag{4.36}$$

which shows that $\lambda_l>\lambda_s$, in qualitative agreement with experiments.

B. Expanding and shrinking domains

A growing or shrinking domain is described by two kink solutions of opposite orientation traveling at different but constant velocities v_L and v_R. The positions of the left and right domain walls are then given by $x_L(t)=x_{L0}+v_Lt$, $x_R(t)=x_{R0}+v_Rt$, respectively. In order to avoid interaction between the domain walls, their distance is taken to be large in comparison with the Landau-Ginzburg length, i.e., $x_R-x_L\gg|\mu|^{-1/2}$. The left kink connects a domain with a small amplitude A_s' at $x=-\infty$ to one with a large amplitude A_l at $x=x_c(t)$ inside the strongly tilted domain, and we assume $x_c-x_L\gg|\mu|^{-1/2}$. Note that at $t=-\infty$ the left kink corresponds to a solution of amplitude A_l. The right kink connects a domain with a large amplitude A_l at $x=x_c$ to one with a small amplitude A_s at $x=\infty$, and $x_R-x_c\gg|\mu|^{-1/2}$, which ensures that the two kink solutions can be viewed as independent. At $t=-\infty$ the right kink corresponds to a solution of amplitude A_s.

Again, we introduce comoving coordinates $X=x-x_{L/R}(t)$. x_c can be effectively replaced by an infinite coordinate, namely by ∞ for the L trajectory and by $-\infty$ for the R trajectory. Requiring

$$\Phi_x^R\xrightarrow[t\to\infty]{}0\ ,$$

we obtain the analog of Eq. (4.7)

$$\Phi_x^R(X)=\frac{\omega}{v_R}\left[A_s-A(X)+\frac{D'}{v_R}A_X\right]\ , \tag{4.37}$$

which for $t\to\infty$ ($\cong X\to-\infty$) approaches $\Phi_x^R(-\infty)=(\omega/v_R)(A_s-A_l)$. For continuity reasons, we must have $\Phi_x^L(\infty)=\Phi_x^R(-\infty)$, which leads to

$$\Phi_x^L(X)=\omega(A_l-A_s)\left[\frac{1}{v_L}-\frac{1}{v_R}\right]+\frac{\omega}{v_L}\left[A_s-A(X)+\frac{D'}{v_L}A_X\right]\ . \tag{4.38}$$

Inserting these expressions into (4.1), we obtain for the right kink

$$A_{XX}+\left[v_R+\left[\gamma+\rho_R\frac{D'}{v_R}\right]A\right]A_X+\frac{dU_R}{dA}=0\ , \tag{4.39}$$

$$U_R(A)=-\tfrac{1}{4}A^4-\tfrac{1}{3}\rho_RA^3+\tfrac{1}{2}\bar{\mu}_RA^2+\nu A+\text{const}\ , \tag{4.40}$$

$$\rho_R=\frac{\epsilon\omega}{v_R},\quad \bar{\mu}_R=\mu+\rho_RA_s\ , \tag{4.41}$$

and for the left kink

$$A_{XX}+\left[v_L+\left[\gamma+\rho_L\frac{D'}{v_L}\right]A\right]A_X+\frac{dU_L}{dA}=0\ , \tag{4.42}$$

$$U_L(A)=-\tfrac{1}{4}A^4-\tfrac{1}{3}\rho_LA^3+\tfrac{1}{2}\bar{\mu}_LA^2+\nu A+\text{const}'\ , \tag{4.43}$$

$$\rho_L=\frac{\epsilon\omega}{v_L},\quad \bar{\mu}_L=\mu+\rho_LA_s+\epsilon\omega(A_l-A_s)\left[\frac{1}{v_L}-\frac{1}{v_R}\right]\ . \tag{4.44}$$

A_l is a common maximum of U_R and U_L. A_s and A_s' are also maxima of U_R and U_L, respectively, but $A_s=A_s'$ only if either $v_R=v_L$ or $A_s=0$.

In order to obtain analytic results we assume that the velocities v_R and v_L deviate only slightly from v^*, due to a small deviation of μ from μ^*. Furthermore, we assume that the *shapes* of the trajectories remain unchanged, i.e., that they only change via their parameters. We set

$$A(X)=\tfrac{1}{2}(A_l-A_s)Z_R(X)+\tfrac{1}{2}(A_l+A_s)\ , \tag{4.45}$$

$$Z_R(X)=-\tanh\frac{1}{\sqrt{2}}A^+X \tag{4.46}$$

for the right trajectory and

$$A(X)=\tfrac{1}{2}(A_l-A_s')Z_L(X)+\tfrac{1}{2}(A_l+A_s')\ , \tag{4.47}$$

$$Z_L(X)=\tanh\frac{1}{\sqrt{2}}A^+X \tag{4.48}$$

for the left one.

Then the Fredholm condition analogous to (4.20) becomes, for the R trajectory, after integration

$$U_R(A_s)-U_R(A_l)+\frac{\sqrt{2}}{6}\left[v_R+\frac{1}{2}\left[\gamma+\rho_R\frac{D'}{v_R}\right]\times(A_l+A_s)\right]\times(A_l-A_s)^2A^+=0\ . \tag{4.49}$$

We now expand U_R, the amplitudes A_l and A_s, and the parameters $\bar{\mu}_R$, v_R, and ρ_R to first order in their deviations from the Maxwell point. Setting $\delta\mu_R=\bar{\mu}_R-\bar{\mu}^*$, $\delta v_R=v_R-v^*$, $\delta A_1=A_s-A_1$, and $\delta A_3=A_l-A_3$, we can write the result as follows:

$$-\tfrac{1}{2}\delta\mu_R+\frac{1}{2}\frac{\delta v_R}{v^*}(A_1^2+A_1A_3+A_3^2)$$
$$+\frac{\sqrt{2}}{6}\frac{A_3-A_1}{A_1+A_3}A^+\left[\frac{\delta v_R}{v^*}[3v^*+\gamma(A_1+A_3)]-v^*\frac{\delta A_1+\delta A_3}{A_1+A_3}\right]=0\ . \quad (4.50)$$

A comparison with the results of Caroli, Caroli, and Fauve [14] is most easily done at this point. If we set $\nu=0$, we obtain $A_1=0$, $\delta A_1=0$, $A_3=A^*=2A^+$, $\delta A_3=\delta A^*$, $\mu_R=\mu$, $\delta\mu_R=\delta\mu$. Since $A^*=(2|\mu^*|)^{1/2}$, this leads to

$$-\frac{1}{2}\frac{\delta\mu}{|\mu^*|}+\frac{\delta v_R}{v^*}+\frac{1}{6(|\mu^*|)^{1/2}}\left[\frac{\delta v_R}{v^*}(3v^*+\gamma A^*)=v^*\frac{\delta A^*}{A^*}\right]=0\ , \quad (4.51)$$

an expression which agrees with the result of Ref. [14], if the δA^* term is neglected. However, it is difficult to see any justification for such an approximation, because in general this term is of the same order of magnitude as the others as we shall see below. (In the expansion of the potential, δA^* terms cancel exactly, because the expansion is about a maximum. But the expansion of the dissipative term yields contributions from the variation of A^*.)

Using the fact that both A_s and A_l are roots of dU_R/dA, we can express δA_1 and δA_3 in terms of $\delta\mu_R$ and $\delta v_R/v^*$,

$$\frac{\delta A_1+\delta A_3}{A_1+A_3}=\frac{1}{2(A^+)^2}\left[\delta\mu_R-\frac{3}{2}\frac{\delta v_R}{v^*}(A_1^2+A_3^2)\right]\ . \quad (4.52)$$

Furthermore,

$$\delta\mu_R=\frac{\delta\mu}{1-[\rho^*A_1/2(A^+)^2]}-A_1\rho^*\frac{\delta v_R}{v^*}\ . \quad (4.53)$$

Inserting these expressions into (4.50) and using (4.20) we arrive after some algebra at

$$\frac{\delta\mu}{2|\tilde{\mu}|}\left[1+\frac{v^*}{\sqrt{2}|\rho^*|}\right]=\frac{\delta v_R}{v^*}\left[1-\frac{1}{4(A^+)^2}\left[9\frac{\nu}{\rho^*}-A_1\rho^*\right]\right]\left[1+\frac{v^*}{\sqrt{2}|\rho^*|}\right]+\frac{v^*}{\sqrt{2}|\rho^*|}\left[2+\tfrac{1}{3}\rho^{*2}\frac{l_\Phi^*}{v^*}\right]\Bigg], \quad (4.54)$$

where $|\tilde{\mu}|=2(A^+)^2-A_1\rho^*=|\mu^*|+9(\nu/\rho^*)-2A_1\rho^*=|\mu^*|+O(\nu^2)$ and $l_\Phi^*=D'/v^*$. An analogous calculation for the left kink yields

$$\frac{\delta\mu}{2|\tilde{\mu}|}\left[1-\frac{v^*}{\sqrt{2}|\rho^*|}\right]=\frac{\delta v_L}{v^*}\left\{1-\left[\frac{|\rho^*|}{2A^+}+\frac{1}{4(A^+)^2}\left[9\frac{\nu}{\rho^*}-A_1\rho^*\right]\right]\left[1-\frac{v^*}{\sqrt{2}|\rho^*|}\right]-\frac{v^*}{\sqrt{2}|\rho^*|}\left[2+\tfrac{1}{3}\rho^{*2}\frac{l_\Phi^*}{v^*}\right]\right\}+\frac{\delta v^R}{v^*}\frac{|\rho^*|}{2A^+}\left[1-\frac{v^*}{\sqrt{2}|\rho^*|}\right]\ . \quad (4.55)$$

Equations (4.54) and (4.55) are the central result of this section. In the written form they hold for any sign combination of ρ and ν.

In order to analyze the structure of these relations in more detail, we introduce some abbreviations and rewrite them as

$$\frac{\delta\mu}{2|\tilde{\mu}|}(1+\beta_1)=\frac{\delta v_R}{v^*}(1+\beta_2)\ , \quad (4.56)$$

$$\frac{\delta\mu}{2|\tilde{\mu}|}(1-\beta_1)=-\frac{1}{2}\frac{\delta v_L}{v^*}(1+\beta_3)+\frac{3}{2}(1+\delta)\frac{\delta v_R}{v^*}(1-\beta_1)\ , \quad (4.57)$$

then we calculate the coefficients to linear order in ν (up to this point we did not use the smallness of ν). The result of Caroli, Caroli, and Fauve is obtained from (4.56) and (4.57) by setting $\nu=0$ and $\beta_1=0$; the smallness of the latter quantity is not granted, in general. Our β_2 corresponds to their β, β_3 reduces to 2β within their approximation, and δ becomes zero.

We obtain

$$\beta_1=\frac{v^*}{\sqrt{2}|\rho^*|}\ , \quad (4.58)$$

$$\delta=\frac{3\nu}{\mu^*\rho^*}+O(\nu^2)\ , \quad (4.59)$$

$$\beta_2=\beta_1(2+\tfrac{1}{3}\chi)+(1+\beta_1)\frac{3\delta}{4}+O(\nu^2)\ , \quad (4.60)$$

$$\beta_3=\beta_1(2+\tfrac{2}{3}\chi)+(1-\beta_1)\frac{3\delta}{2}+O(\nu^2)\ , \quad (4.61)$$

where $\chi=\rho^{*2}(l_\Phi^*/v^*)$. The coefficients β_1, β_2, β_3, and χ are positive, whereas δ can have either sign. Written in terms of these coefficients, (4.56) reads

$$\frac{\delta v_R}{v^*}=\frac{\delta\mu}{2|\bar{\mu}|}\frac{1+\beta_1}{1+\beta_2} \tag{4.62}$$

and the combination of (4.56) and (4.57) gives

$$\frac{\delta v_R-\delta v_L}{\delta v_R}=\frac{4\beta_1(1+\frac{1}{3}\chi)}{(1+\beta_1)(1+\beta_3)}\ . \tag{4.63}$$

The factor of $\delta\mu$ on the right-hand side of (4.62) and the right-hand side of (4.63) are positive. Hence we have shown that δv_R and $\delta v_R-\delta v_L$ both have the same sign as $\delta\mu$. This means that close to the Maxwell point μ^*, i.e., when the pulling velocity is close to V^* or, equivalently, the wavelength of the basic weakly tilted pattern is close to λ^*, growing domains of a strongly tilted state can propagate into the weakly tilted one for $V^*<V\ (<V_c)$. Domains with $V<V^*$ are also possible but they will shrink and probably disappear eventually. The opening angle between the walls of these domains in a space-time portrait [22] is uniquely determined by the four parameters defined above.

While the sign of δv_R is always the same as that of $\delta\mu$, the sign of δv_L changes to opposite that of $\delta\mu$ in a certain region of β_1 values, i.e., an increase in $\delta\mu$ will always accelerate the front wall of the domain but sometimes decelerate the back wall, and a decrease in $\delta\mu$ will sometimes accelerate the back wall.

Inside the strongly tilted domain, the wavelength of the pattern is always larger than outside, since $\Phi_X<0$ [see Eq. (4.37)]. After the system has been swept by a strongly tilted inclusion, both its amplitude and its wavelength have changed. The amplitude, which was A_s before the arrival of the "tilt wave" is A_s' afterwards. In order to get an idea about the change of the wavelength, we recall that at time $t=-\infty$ the gradient Φ_x of the phase equals zero at any fixed locus on the pattern [see Eq. (4.37)]. With the arrival of the front kink, Φ_x starts to change, and in the wake of the kink, it approaches the value $\Phi_x^R(-\infty)=(\omega/v)(A_s-A_l)$ which is negative. Then the left kink arrives, increasing Φ_x again, and after it has left, the phase gradient behind it approaches $\Phi_x^L(-\infty)=(\omega/v_L)(A_l-A_s')-(\omega/v_R)(A_l-A_s)$ [see Eq. (4.38)]. The change in local wave number caused by the passage of the strongly tilted pattern is equal to the total change of Φ_x which is given by $\Phi_x^L(-\infty)-\Phi_x^R(\infty)=\Phi_x^L(-\infty)$. Expanding about the Maxwell point again, we obtain

$$\Phi_x^L=\xi\delta\mu\ . \tag{4.64}$$

Herein,

$$\xi=\frac{3}{|\epsilon|[1+27(\nu/\rho^{*3})]^{1/2}}\frac{2\beta_1(1+\frac{1}{3}\chi)}{(1+\beta_2)(1+\beta_3)}\ , \tag{4.65}$$

which is obviously positive. Hence the wavelength decreases when $\delta\mu$ is positive (because its change is opposite to that of Φ_x) and increases when $\delta\mu$ is negative. Since μ is a monotonously *increasing* function of the wavelength, its value is driven towards μ^*. Therefore, shrinking or growing domains act as *wavelength selectors* and the *dynamically selected wavelength* of the weakly tilted structure is λ_*. Of course, these ideas do not provide any insight into the selection mechanism *above* the "critical point."

C. Preferred direction of the tilt angle

In the discussion of inequality (4.16), we have seen that there are two types of bifurcations which allow the coexistence of weakly and strongly tilted domains below $\bar{\mu}=0$. They are depicted in Figs. 10 and 11, respectively. When ν and ρ have opposite signs (Fig. 11), the bifurcation has a subcritical branch, while for equal signs of ν and ρ there is no such structure (Fig. 10). Our analysis applies to both cases, i.e., there is a Maxwell point and growing or shrinking domains are possible in both situations.

For a given eutectic grain, ν should be considered fixed, i.e., to have a definite sign, determined by the relation between crystallographic orientation and pulling direction. However, the sign of ρ changes with that of the traveling domain's velocity. For example, for positive ν and ω, domains traveling to the right ($\rho<0$) should be describable based on the bifurcation picture of Fig. 11. Domains traveling to the left then have a bifurcation as shown in Fig. 10, with A replaced by $-A$. In the first case, the amplitude of the strongly tilted state has the same sign as that of the basic (weakly tilted) state, in the second the amplitudes—or tilt angles—have opposite signs.

The question is then which of the two situations is more likely to occur in a typical experiment. Localized inclusions of strongly tilted domains can be produced experimentally by a sudden increase of the pulling velocity which is, however, not large enough to carry the system into the region (above $\bar{\mu}=0$) where *extended* tilted domains exist. But even if such a velocity jump results in a value of $\bar{\mu}$, for which weakly and strongly tilted states can coexist, there is *a priori* no reason for the system to tilt strongly, since the weakly tilted state is still linearly stable.

However, when the bifurcation has a subcritical part, a local wavelength fluctuation may increase the wavelength and, accordingly, $\bar{\mu}$ by so much that the system is forced into the region [of order $O(\sqrt{|\nu|})$ about $\bar{\mu}=0$, see Fig. 11] where only a strongly tilted state is possible. Such a fluctuation will most likely occur in the vicinity of a grain boundary. Let us assume that during the tilting transition the wavelength remains essentially unchanged. Now the wavelength corresponding to a certain $\bar{\mu}$ value of the weakly tilted state is equivalent to a *lower* value of $\bar{\mu}$ in the strongly tilted state, since the "natural" wavelength of a strongly tilted state is larger than that of a weakly tilted one. Hence, once the localized inclusion is created, its $\bar{\mu}$ value drops back into the coexistence region. There is no comparable mechanism in the case of Fig. 10, where the system always has the choice to stay on the lower branch when the pulling velocity is changed. Even though in principle strongly tilted coexisting states are possible, their creation is not likely in the described type

of experiment. Intuitively this is clear—such a process would require a change of the tilt direction. We then conclude that, given the orientation of the underlying eutectic grain, one should expect that localized inclusions preferentially tilt in the same direction as the basic state, and that the dynamically created bifurcation is generically of the type indicated in Fig. 11.

This argument refers only to the *creation* of strongly tilted domains. An *existing* tilted domain that travels across a grain boundary into a grain with opposite crystalline orientation may continue to exist. Depending on the parameter values it may then shrink or expand. If the basic pattern on both sides of the grain boundary is already at its dynamically selected wavelength and if all parameters but ν are the same on both sides, then a constant-width tilted domain that moves from a matrix of the same tilt orientation into one with the opposite orientation will shrink there. This can be concluded from (4.24) which shows that $\bar{\mu}^*$ is *smaller* when ν and ρ have an opposite sign than otherwise. Hence a domain existing at the Maxwell point before crossing the grain boundary will have a $\bar{\mu}$ value below the Maxwell point after the crossing.

Of course, the representation of anisotropy by a single parameter is an oversimplification. (In the full model, anisotropy is described by six parameters.) Therefore, our conclusions are not rigorous statements, but rather plausibility arguments.

V. CONCLUSIONS

We have treated the coupling between the spontaneous parity-breaking transition, which results from a kinetic instability, and the crystalline anisotropy. The effect of crystalline anisotropy on front dynamics and pattern selection has been revealed to play an important role, as often reported in the metallurgical literature. In recent experiments [13] on the transparent CBr_4-C_2Cl_6 eutectic alloy, the correlation between crystal orientations and the tilt of lamellae has been carefully analyzed. It has emerged from this analysis that the so-called "symmetric" state is in reality slightly tilted due to the orientation of the grain along some crystallographic direction that usually deviates from the growth axis.

Many natural questions, such as how does the supercritical pitchfork bifurcation [8] change in the presence of crystalline anisotropy, why do only tilted domains with a preferential direction expand in a given grain, and how does the coupling of the phase to the amplitude of a finite-width domain of tilted lamellae modify the overall picture of the bifurcation diagram, had remained unanswered.

For the generic case where the direction of minimal surface energy makes a nonzero angle with the growth axis, we have shown from elementary considerations that for tilted lamellae filling the whole front, the effect of anisotropy is a destruction of the pitchfork bifurcation and its replacement by an imperfect bifurcation. We have pointed out the analogy between this problem and a second-order ferromagnetic transition in the presence of an external magnetic field. The imperfect character of the bifurcation has been confirmed by numerical solution of the front integral equation. The turning point of the lower branch of the imperfect bifurcation diagram (Fig. 8) lies at a distance of the order of $|\nu|^{2/3}$ from the critical point of the original pitchfork bifurcation. Therefore in order to achieve the possibility for tilted lamellae filling the whole front to be in the state corresponding to that branch, one should impose a velocity jump higher than the one expected in the anisotropy-free case [8], otherwise the extended parity-broken state lying on the upper branch will be favored in general. If the velocity jump is not large enough, however, one often observes domains of finite widths that either expand or shrink according to the magnitude of the velocity jump. Here again most of these domains are observed to be tilted in a favorable direction. We have analyzed the coupling of the amplitude and the phase in a picture *à* la Coullet, Goldstein, and Gunaratne [10]. From a pedestrian analysis we have shown that this coupling either transforms the imperfect bifurcation into a subcritical one (Fig. 11), provided that the strength of the crystalline anisotropy is not too large, or into a bifurcation of the type shown in Fig. 10. We have determined the Maxwell-like point where the basic state (but pinned on the preferential crystalline orientation) coexists with the strongly tilted one.

It is worth pointing out that in all this treatment no hint emerges of the existence of stable localized states, or solitons. Indeed the present results simply state (i) that a coexistence of the two states is possible despite the imperfect character of the homogeneous bifurcation owing to the coupling of the phase and the amplitude, (ii) in the metastability domain of the phase-amplitude-induced subcritical bifurcation the strongly tilted state either expands or collapses, according to whether the control parameter lies above or below the Maxwell point, in a manner similar to that of a nucleation process of a droplet in a gas. The question whether a coupling of the amplitude and the phase may cause the appearance of a localized tilted state that travels in a shape-preserving manner for a finite band inside the metastability domain (what we should legitimately call soliton) requires further investigation.

Finally another point worth mentioning is that the homogeneous solution of (4.1) and (4.2) ($A=\text{const}$ and $\Phi=\text{const}\times t$) suffers long-wavelength instabilities, as first pointed out by Fauve, Douady, and Thual [23]. It is therefore important to see whether the extended tilted domains recently observed by Faivre, Guthmann, and Mergy [12] are really stable, as these experiments seem to indicate, or whether they are rather very long transients before a long-wavelength instability prevails, and if so what type of structures would then emerge. Of course an amplitude and phase expansion, from which the conclusion about stability follows, is by its very nature valid close enough to the threshold only. We know in solidification problems, however, that even if the operating point is close to the critical one, strong nonlinearities are present that usually escape amplitude expansions.

This is traced back to the disparate character of the two competing scales, associated with the stabilizing capillary forces and the destabilizing mass diffusion. It is therefore imperative, in order to obtain conclusive answers, to perform a full stability analysis of the homogeneous asymmetric states from the "microscopic" equations of growth. This should constitute a crucial step towards a deeper understanding of the various dynamical manifestations of solidification fronts.

ACKNOWLEDGMENTS

A considerable part of this work was completed during a stay of both authors at the Aspen Center for Physics. We are most grateful for the hospitality of, and the enjoyable atmosphere at, the Center. K.K. acknowledges a useful discussion with C. Caroli. C.M. acknowledges financial support from the Centre National d'Etudes Spatiales.

[1] J. D. Hunt and K. A. Jackson, Trans. Metall. Soc. AIME **236**, 843 (1966).

[2] V. Seetharaman and R. Trivedi, Metall. Trans. **19A**, 2955 (1988).

[3] W. Kurz and D. J. Fisher, *Fundamentals of Solidification* (Trans. Tech. Publ., Aedermannsdorf, 1984).

[4] R. Racek, Thèse d'Université, Nancy I, 1973; H. E. Cline, Mater. Sci. Eng. **65**, 93 (1984).

[5] A. J. Simon, J. Bechoefer, and A. Libchaber, Phys. Rev. Lett. **61**, 2574 (1988).

[6] G. Faivre, S. de Cheveigné, C. Guthmann, and P. Kurowski, Europhys. Lett. **9**, 779 (1989).

[7] K. Kassner and C. Misbah, Phys. Rev. Lett. **65**, 1458 (1990); **66**, 522(E) (1991).

[8] K. Kassner and C. Misbah, Phys. Rev. A **44**, 6533 (1991).

[9] M. Rabaud, S. Michalland, and Y. Couder, Phys. Rev. Lett. **64**, 184 (1990).

[10] P. Coullet, R. Goldstein, and G. H. Gunaratne, Phys. Rev. Lett. **63**, 1954 (1989).

[11] H. Levine and W. J. Rappel, Phys. Rev. A **42**, 7475 (1990).

[12] G. Faivre, C. Guthmann, and J. Mergy (private communication).

[13] B. Caroli, C. Caroli, G. Faivre, and J. Mergy, J. Cryst. Growth **118**, 135 (1992).

[14] B. Caroli, C. Caroli, and S. Fauve, J. Phys. I (Paris) **2**, 281 (1992).

[15] K. Kassner and C. Misbah, Phys. Rev. A **44**, 6513 (1991).

[16] H. Müller-Krumbhaar, T. Burkhardt, and D. Kroll, J. Cryst. Growth **38**, 13 (1977).

[17] The authors of Ref. [13] have termed eutectic grains "floating" in which regular growth prevails (the orientation of lamellae is almost parallel to the pulling direction) and distinguish them from the less abundant "locked" grains where large tilt angles having no dynamical origin can exist.

[18] K. Kassner and C. Misbah, Phys. Rev. Lett. **66**, 445 (1991).

[19] K. Kassner and C. Misbah, J. Phys. A (to be published).

[20] In order to obtain the amplitudes of the homogeneous infinitely extended states of the system, one has to require $A_\infty = A = \text{const}$ in Eq. (4.11), which yields the known solutions $A = 0$, $A = \pm\sqrt{\mu}$ (for $\nu = 0$).

[21] *Handbook of Mathematical Functions,* edited by M. Abramowitz and I. A. Stegun (Dover, New York, 1972).

[22] J.-M. Flesselles, A. J. Simon, and A. J. Libchaber, Adv. Phys. **40**, 1 (1991).

[23] S. Fauve, S. Douady, and O. Thual, Phys. Rev. Lett. **65**, 385 (1990).